Materials Science in Semiconductor Processing 17 (2014) 13–20

Contents lists available at ScienceDirect

Materials Science in Semiconductor Processing

journal homepage: www.elsevier.com/locate/mssp

Investigation of structural and optoelectronic properties of annealed nickel phthalocyanine thin films

Mina Neghabi *, Mehdi Zadsar, Seyed Mohammad Bagher Ghorashi

Department of Physics, Faculty of Sciences, Najafabad Branch, Islamic Azad University, Isfahan, Iran

ARTICLE INFO

Keywords:
Organic semiconductors
Metal-substituted phthalocyanine
Schottky barriers
Charge transport
Thermal evaporation

ABSTRACT

Thin films of nickel phthalocyanine (NiPc) were prepared by thermal evaporation and the effects of annealing temperature on the structural and optical properties of the samples were studied using different analytical methods. Structural analysis showed that the grain size and crystallinity of NiPc films improved as annealing temperature increased from 25 to 150 °C. Also, maximum grain size (71.3 nm) was obtained at 150 °C annealing temperature. In addition, NiPc films annealed at 150 °C had a very smooth surface with an RMS roughness of 0.41 nm. Optical analysis indicated that band gap energy of films at different annealing temperatures varied in the range of 3.22–3.28 eV. Schottky diode solar cells with a structure of ITO/PEDOT:PSS/NiPc/Al were fabricated. Measurement of the dark current density–voltage (*J–V*) characteristics of diodes showed that the current density of films annealed at 150 °C for a given bias was greater than that of other films. Furthermore, the films revealed the highest rectification ratio (23.1) and lowest barrier height (0.84 eV) demonstrating, respectively, 23% and 11% increase compared with those of the deposited NiPc films. Meanwhile, photoconversion behavior of films annealed at 150 °C under illumination showed the highest short circuit current density (0.070 mA/cm^2) and open circuit voltage of (0.55 V).

1. Introduction

In recent years, a large family of phthalocyanines (Pcs) such as CuPc [1], SnPc [2], PbPc [3], FePc [4], CoPc [5], MgPc [6] and ZnPc [7,8] have been studied extensively for potential optoelectronic applications. For certain advantages including ease of fabrication, thermal and chemical stability and insolubility in water, compatibility with flexible substrates and low-cost production processing, thin Pc films are commonly used in building electronic and optoelectronic devices such as organic solar cells [9,10], organic light emitting diodes (OLEDs) [11–13], field-effect transistors [14], optical recording [15], photodynamic therapy, non-linear optics [16], catalysis [17] and gas sensors [18]. It is known that the improvement of structural properties and photoconversion performance of PC-based devices rely mainly on understanding and controlling charge injection and charge transport processes [19–21]. It is worth noting that these processes can be affected by various parameters such as the substrate temperature and annealing treatment [1,22]. Hence, it is very important to carefully examine the impacts of annealing temperature on injection and transport characteristics and photoconversion performance of Pc-based devices. In the present research, nickel phthalocyanine (NiPc) was selected among the Pc compounds because of characteristics like high chemical and thermal stability, rather than high charge mobility and reproducibility [23]. However, not much investigation has been conducted into the effects of annealing treatment on the structural, electrical and optical properties of the NiPc thin films.

First, the sandwich-type ITO/PEDOT:PSS/NiPc/Al structure was fabricated by thermal evaporation. Next, the effect of

* Corresponding author. Tel.: +98 3312291111; fax: +98 3312291016.
E-mail address: mina_neghabi@yahoo.com (M. Neghabi).

1369-8001/$ - see front matter © 2013 Elsevier Ltd. All rights reserved.
http://dx.doi.org/10.1016/j.mssp.2013.08.002

annealing temperature in air on structural, morphological and optical properties of NiPc thin films was examined by X-ray diffraction (XRD), scanning electron microscopy (SEM), atomic force microscopy (AFM) and optical transmittance measurements. Also, charge injection and transport characteristics of sandwich organic devices and their junction properties such as ideality factor and barrier height were studied by measuring current–voltage characteristics in dark and under illumination conditions. It was found that for the annealed NiPc films; the structural properties were improved compared to the as-deposited NiPc films. Furthermore, the results demonstrated that phthalocyanines based sandwich organic devices annealed at various temperatures had the enhanced rectification and photoconversion properties.

2. Experimental procedure

The poly-3,4-ethylenedioxythiophene/polystyrenesulphonate (PEDOT:PSS) and Nickel phthalocyanine (NiPc) powder with purity of 98% used in the present study were purchased from Sigma-Aldrich. The structures of the molecules have been shown in Fig. 1(a). The ITO coated glasses with 15 Ω/sq sheet resistance were used as substrates (anode). These anode glasses were cleansed by sonicating in propanol, acetone, ethanol, deionized water and isopropyl alcohol for 10 min and then dried under nitrogen gas flow. A buffer layer of PEDOT:PSS was spin-coated onto the ITO anodes at 3000 rpm and then dried in oven at 110 °C for 30 min. NiPc layer was deposited on the samples using thermal evaporation under 10^{-6} Torr pressure. The film deposition rate was (1 A° s^{-1}) and the thickness of layer was controlled by a quartz vibrating monitor placed near the samples. Different values of film thickness were measured after deposition using a Decktac profiler. Finally the aluminum electrode (cathode) was deposited by thermal evaporation in tungsten boats through an appropriate mask. The temperature of the substrates was close to room temperature (25 °C) during deposition. The resulting area of each device was about 15 mm^2. Fig. 1(b) shows a schematic diagram of the device with the structure of ITO/PEDOT: PSS (40 nm)/NiPc (200 nm)/Al (150 nm). Then, samples have been annealed in air at different temperatures ranging from 70, 100, 120 to 150 °C for 1 h to investigate the influence of annealing on structural, morphological, optical and photovoltaic properties. The optical absorption spectrum of the 200 nm thin film of NiPc layer on a glass slide was recorded by employing a Perkin Elmer double beam spectrophotometer. XRD studies of the NiPc films were applied using Philips 40 kV, 30 mA, Cu Kα radiation system with wavelength of 1.54 Å in the scan range of 2θ between 2° and 45° with a step size of 0.05 (2θ/s). The microstructure of films was examined by SERON Technology (AIS 2100) SEM on 20 kV operating voltage. The surface morphology of NiPc films was also monitored by an atomic force microscope (AFM, Model DS-95-200E). Photovoltaic characterization was performed with a Keithley 2400 source-meter and Oriel Sol1A Class ABB solar simulator (100 mW/cm^2).

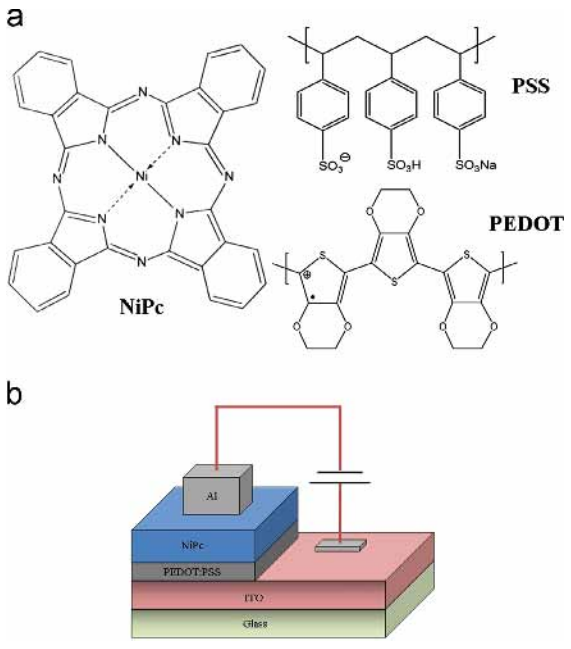

Fig. 1. (a) The chemical structures of NiPc and PEDOT:PSS and (b) Schematic structure of schottky diode solar cell.

3. Results and discussion

3.1. Characteristics of deposited NiPc films

3.1.1. X-ray diffraction

The X-ray diffraction patterns of NiPc powder and 200 nm thick NiPc films were deposited on glass at room temperature (25 °C) and then were annealed at different temperatures in air (Fig. 2). We know that phthalocyanines usually have two typical crystalline polymorphous structures: metastable α- and stable β-phases [24]. XRD analysis revealed that the NiPc powder was as a mixture of both α-form and β-form. However, as it is clear in Fig. 2, thin films deposited at room temperature and annealed at various temperatures are in the α-phase and there is only a significant peak around (2θ=6.9°) along the (001) direction which can be identified as the (200) reflection of

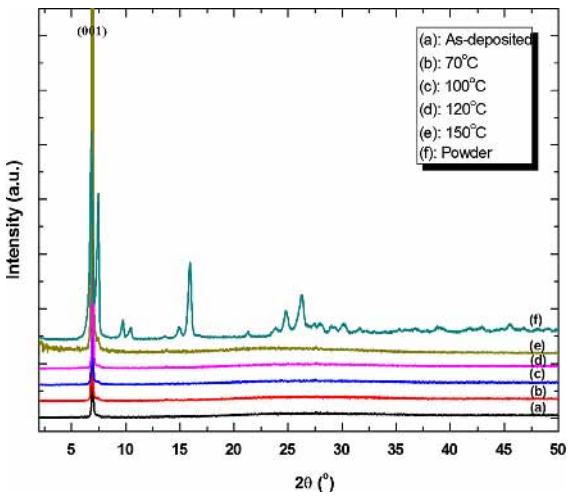

Fig. 2. XRD patterns of the NiPc thin films annealing at various temperatures.

tetragonal α-NiPc. The results were in good agreement with the previous literature works [25]. It was found that there was a direct correlation between the intensity and sharpening of the predominant peak and annealing temperature. This result indicated that crystallinity and lattice quality of the films improved with annealing treatment. The crystallinity improvement can be attributed to the destruction of pseudomorphic layers present in the film and increased the ability of atoms to move towards stable sites in the lattice. In order to investigate the influence of annealing treatment on mean crystallite size of NiPc thin films, the mean crystallite size of NiPc was calculated by Scherrer's relation [26]:

$$G = \frac{0.9\lambda}{\beta \cos\ \theta} \quad (1)$$

where G is the crystallite size, λ (1.548 °A) is the wavelength of X-ray radiation, β is the full width at half maximum (FWHM) of the diffraction peak and θ is the Bragg diffraction angle of the XRD peak.

The mean crystallite sizes of the as-deposited NiPc thin film and annealing with various temperatures were calculated and shown in Table 1. It can be seen that the mean crystallite size growth of NiPc is a function of annealing temperature increasing from 49.8 to 71.3 nm. Increased annealing temperature provides sufficient thermal energy for atoms rearrangement, resulting in improving mobility of atoms and consequently in faster crystallite growth. As the crystallite size grows, the pseudomorphic layers formed at room temperature are destroyed by heat treatment and the crystallinity of films improves. It is clear that the quality of films can be improved by decreasing the strain and dislocation.

3.1.2. Electron microscopy

Scanning electron microscopy (SEM) was used to study the microstructure changes of NiPc films annealed at different temperatures. Fig. 3a–e exhibits the SEM images of the films as-deposited and annealed at 70, 100, 120 and 150 °C respectively. It can be seen that as annealing temperature increases the mean crystallite size becomes larger, the surface topography of NiPc films improves and films become more continuous. This behavior can be explained as follows: when annealing temperature increases, the nucleation and growth process also alter, crystallization process improves resulting in growing the mean crystallite size [27]. The result also supports the crystallite size result obtained by XRD earlier which shows the crystallite becoming larger as the annealing temperature increases.

Table 1
Calculated structural and optical parameters of the NiPc thin films at various annealing temperatures.

Annealing temperature (°C)	Particle size (nm)	RMS roughness (nm)	Band gap energy (eV)
25	49.8 ± 0.3	9.51 ± 0.01	3.28 ± 0.02
70	51.1 ± 0.3	6.33 ± 0.01	3.26 ± 0.02
100	66.7 ± 0.3	4.74 ± 0.01	3.25 ± 0.02
120	70.2 ± 0.3	1.86 ± 0.01	3.23 ± 0.02
150	71.3 ± 0.3	0.41 ± 0.01	3.22 ± 0.02

Experimental errors in temperature $\Delta T = \pm 1$ °C.

3.1.3. AFM analysis

It is obvious that the surface morphological properties of phthalocyanine films used in photovoltaic devices can affect the electrical characteristics and performance of these devices [28]. Hence, it is interesting to investigate the effect of the annealing treatment on the surface morphology of NiPc thin films. Three-dimensional AFM micrographs of NiPc films, each 200 nm thick, annealed at different annealing temperatures as shown in Fig. 4a–e. The AFM images clearly indicate the roughness variations of the NiPc films before and after annealing at four different temperatures. The AFM results reveal that as annealing temperature increases crystallite size grows and larger grains start to form in NiPc thin film annealed at 150 °C compared to those of formed in other films. This also confirms previous results. The root-mean-square (RMS) roughness of NiPc films annealed at different annealing temperatures has been reported in Table 1. It can be seen that the surface roughness of the NiPc films is sensitive to annealing treatment and there is a direct correlation between RMS roughness and film annealing temperature. The 3D surface topography of film annealed at 150 °C (Fig. 4e) was clearly seen to be the smoothest. The 3D surface topography of film annealed at 120 °C (Fig. 4d) was also relatively smooth, and the valleys on the surface were much shallower than those of films annealed at 100 °C and 70 °C (Fig. 4c and b). The surfaces of these samples had valleys with a moderate depth, and as-deposited film (Fig. 4a) had the deepest valleys. In other words, annealing treatment improves the surface smoothness of NiPc film and the adhesion between this layer and the cathode [29].

It is worthwhile mentioning here that, the presence of included defects, such as subparticles and pinholes at interface between phthalocyanine film and other layer, decrease charge carrier injection and thus critically degrade the Schottky diode's performance. Thermal annealing of NiPc films at 70–150 °C resulted in elimination of structural defects and information of high-quality, continuous and uniform films. Consequently, the enhanced Schottky diode's performance may result from the improved surface smoothness of annealed NiPc films.

3.1.4. Estimation of the optical band gap

Fig. 5 shows the variations of absorption coefficient as a function of wavelength in the range 300–900 nm for NiPc films annealed at different temperatures.

It was revealed that all NiPc films showed absorption coefficient patterns without a considerable change with respect to the annealing treatment. It can be seen that there is an absorption peak at wavelength of 330 nm which represents the $\pi \rightarrow \pi^*$ transition corresponding to an intense B band (Soret band). The Soret band gives the fundamental absorption edge. Also there are two peaks at wavelengths of 620 and 674 nm corresponding to an intense Q band which gives the onset energy [30]. It is clear that as the annealing temperature of NiPc thin films increases, intensity of absorption maxima observed at 620 nm increases faster than that

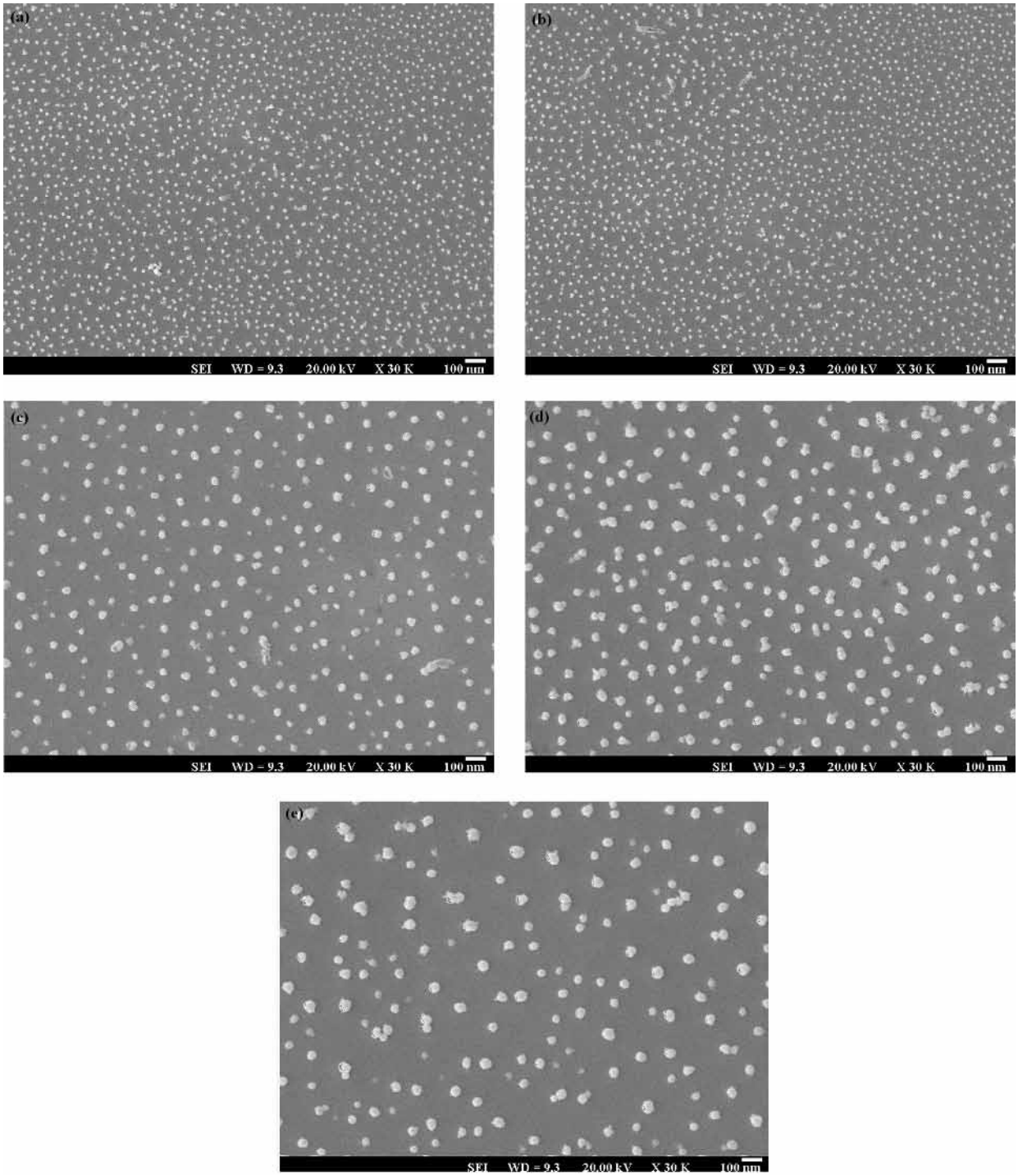

Fig. 3. SEM images of the NiPc thin films at different annealing temperatures ((a) as-deposited, (b) 70 °C, (c) 100 °C, (d) 120 °C and (e) 150 °C).

of peak at 674 nm. Some researchers have reported that absorption peaks at wavelengths of 620 and 674 nm correspond to dimer and monomer phthalocyanine respectively [31]. So, this result reveals the correlation rate between the dimer phthalocyanine and annealing treatment. When the annealing temperature increases, the monomers of NiPc films transformed to aggregates and consequently the dimerization process enhances [32].

The optical band gap values with respect to B bands (Soret bands) were calculated based on the analysis of the fundamental absorption edge by assuming a direct allowed transition between the edges of the ground state π

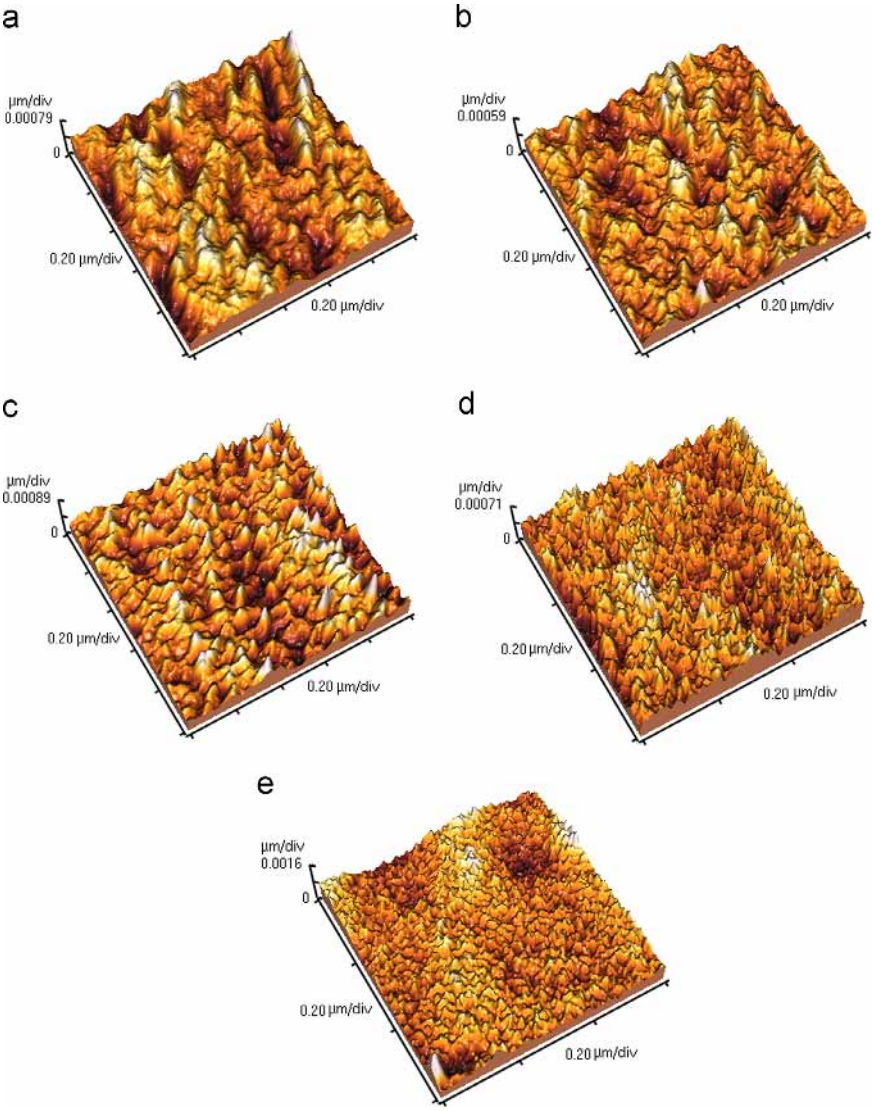

Fig. 4. Three-dimensional AFM images of the NiPc thin films at different annealing temperatures ((a) as-deposited, (b) 70 °C, (c) 100 °C, (d) 120 °C and (e) 150 °C).

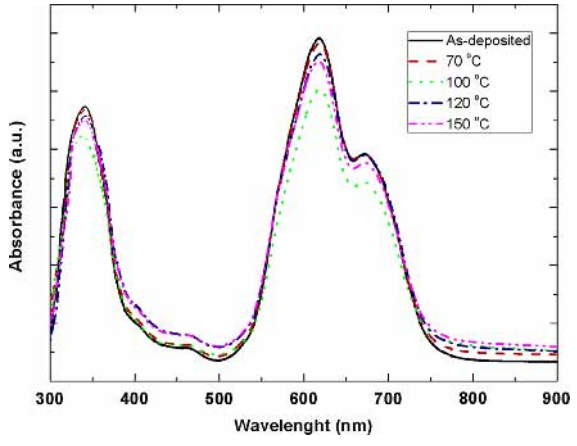

Fig. 5. The absorption spectra for NiPc thin films deposited at different annealing temperatures.

and the π^* in the 300–450 nm range, using the equation [33]

$$(\alpha h\upsilon)^2 = A(h\upsilon - E_g) \quad (2)$$

where α is the absorption coefficient, E_g is energy gap, $h\upsilon$ is the photon energy and A is a constant. The plots of $(\alpha h\upsilon)^2$ versus $h\upsilon$ have a linear region and extrapolation of the straight line to zero absorption gives the energy gap for NiPc films, as-deposited and annealed at different temperatures. The values of E_g for all treatment regimes have been listed in Table 1. As it can be seen when annealing temperature increases up to 120 °C the band gap energy decreases and then varies only slightly if temperature increases still further (Fig. 6).The decrease of the energy gap by the grain size could be caused by the quantum size effects [34]. In fact, the band gap energy decreases due to decreasing grain boundaries and diminishing structural defects. Since grain boundaries and structural defects act as barriers and scattering centers, respectively, for the

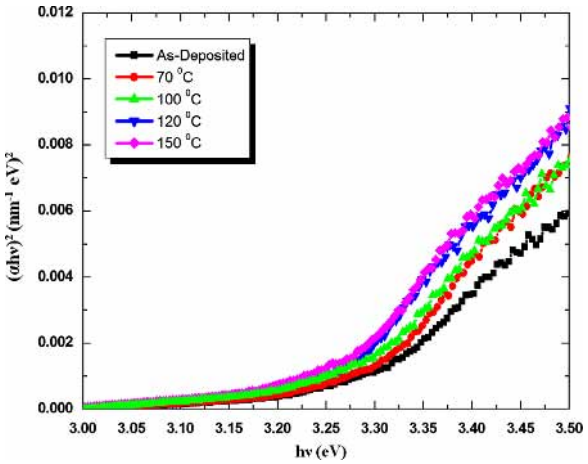

Fig. 6. Variation of the band gap as a function of annealing temperature for NiPc films.

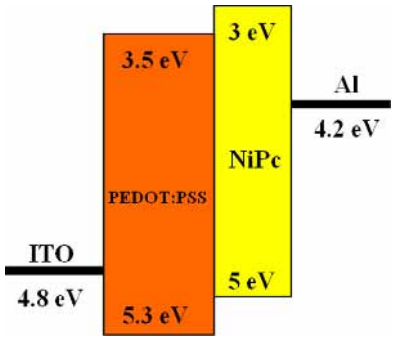

Fig. 7. Energy band diagram of the device with the structure of ITO/PEDOT:PSS (40 nm)/NiPc (200 nm)/Al (150 nm).

cross transport of charge carriers, the reduction of both grain boundaries and defects indicates an improvement in the crystallinity and formation of high quality films. As a consequence, band gap energy decreases.

3.2. Characteristics of fabricated Schottky diodes

In order to investigate the properties of annealed NiPc thin films for their use in organic devices, a series of Schottky diodes with a glass/ITO/PEDOT:PSS/NiPc/Al structure were fabricated. The energy band diagram of the device with the relative alignment of the highest occupied molecular orbital (HOMO) and lowest unoccupied molecular orbital (LOMO) levels of each layer have been shown in Fig. 7. Electrical characteristics of Schottky diodes are given below.

3.2.1. Dark current density–voltage characteristics and transport mechanisms

The dark current density–voltage characteristics of ITO/PEDOT:PSS/NiPc/Al devices for various annealing temperatures have been shown in Fig. 8. It can be seen that annealing temperature affects the current density–voltage characteristics of organic devices. It should be noted that the improved crystallinity and enhanced surface uniformity of

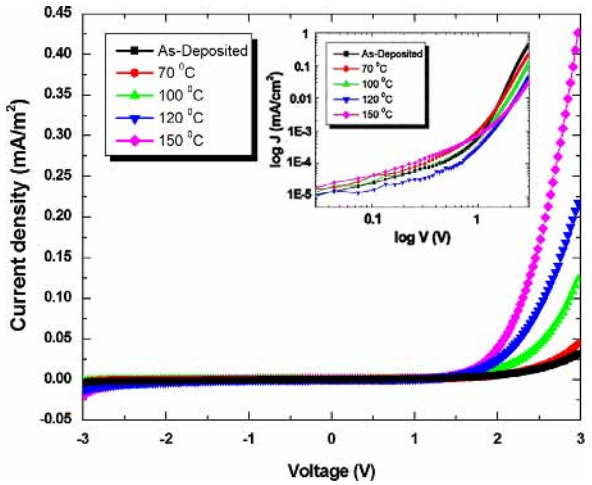

Fig. 8. *J–V* characteristics of glass/ITO/PEDOT:PSS/NiPc/Al Schottky diode solar cells at different annealing temperatures. The inset shows variation of the log *J* versus log *V* at different annealing temperatures.

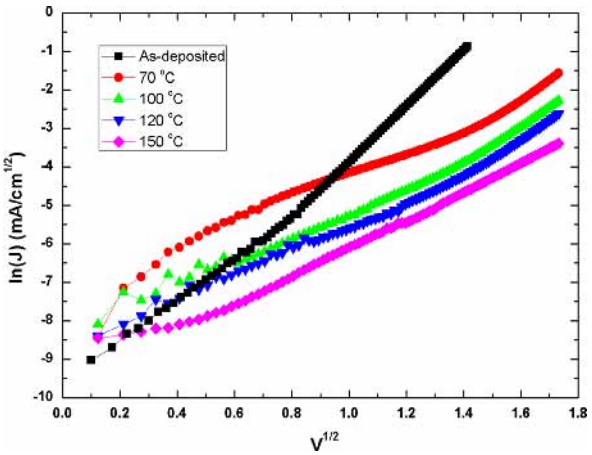

Fig. 9. Semi-logarithmic plot of the forward bias *J–V* characteristic at different annealing temperatures.

annealed NiPc films help to reduce the density of various traps in structures, increase the charge carrier mobility and therefore ultimately facilitate the injection and transportation of the charge carriers. Therefore, it was expected that the current for a given bias was greater for annealed samples than that of as-deposited samples.

To study the transport mechanism of the devices, double logarithmic (log *J* versus log *V*) graph was plotted in the forward bias in the inset of Fig. 8. As observed the double logarithmic characteristic has two distinct linear regions. The first region, low positive bias $V < 1$ V, the slope of the logarithmic characteristic is close to 1 and the conductivity is ohmic (thermionic emission region); in the second region, higher bias range $J \alpha V^m$ where $m \sim 3.99$, 3.95, 3.34, 3.00 and 2.58 for 25, 70, 100, 120 and 150 °C annealing temperature respectively, indicating that there has been a space charge limited current (SCLC) transport mechanism governed by an exponential trap distribution. It is obvious that by increasing annealing temperature, the value of *m* decreases and its value is close to the trap filled

Table 2
Device parameters for NiPc Schottky diodes under dark conditions.

Annealing temperature (°C)	Ideality factor	Barrier height (eV)	Reverse saturation current density (mA/cm^2)	Rectification ratio
25	5.21 ± 0.02	0.93 ± 0.01	0.83	3.1
70	4.70 ± 0.02	0.91 ± 0.01	0.78	6.2
100	4.47 ± 0.02	0.87 ± 0.01	0.68	15.4
120	3.34 ± 0.02	0.85 ± 0.01	0.66	22.3
150	2.21 ± 0.02	0.84 ± 0.01	0.65	23.1

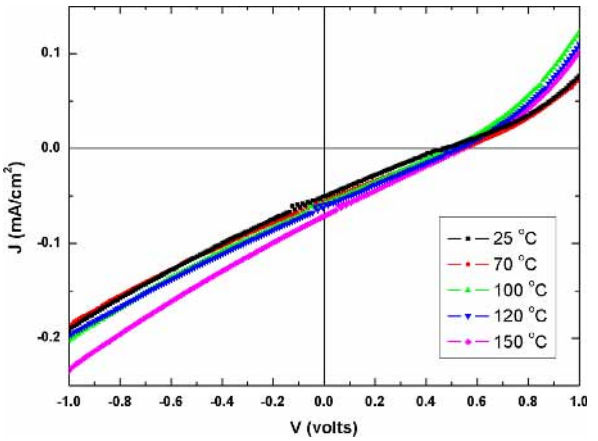

Fig. 10. Current–voltage characteristics of devices with different annealing temperatures under standard illumination at 1 kW/m^2.

limit in SCLC regime ($m=2$) [35]. This is confirmed by structural and morphological results. In fact, it was documented that as annealing temperature increased, a uniform and continuous layer of NiPc was formed so that trapping states of structure decreased and the SCLC regime with filled traps (no trapping) was obtained.

To evaluate the optoelectronic properties of Schottky diodes, the emission mechanism was investigated. Fig. 9, demonstrating J against $V^{1/2}$, shows a linear variation in this region. This type of behavior can be generally attributed to the thermionic emission mechanism that is given by [36]

$$J = J_S\left(\exp\left(\frac{eV}{nkT}\right) - 1\right) \tag{3}$$

where the saturation current, J_s, is given by

$$J_S = A^*T^2\exp\left(-\frac{e\varphi_B}{kT}\right) \tag{4}$$

In the above equation, A^* is the Richardson constant ($A^* = 120$ A/cm^{2}K^2 if the effective mass of electrons inside the dielectric is equal to free electron mass), T is temperature in K, φ_B is the Schottky barrier height at the injecting electrode interface and n is the ideality factor.

The effective values of diode parameters such as ideality factor (n), barrier height (φ_B), rectification ratio (R) and the reverse saturation current density (J_s) were calculated by Eqs. (3) and (4) and were provided in Table 2. It can be seen that annealing temperature plays an important role in optoelectronic properties of devices in the temperature range of 25–120 °C, rectification ratio of devices has increased and barrier height at the electrode–organic interface decreased. It seems that this is due to very good properties of NiPc film-formation through annealing. However, increasing annealing temperature up to 150 °C, NiPc films become approximately saturated in terms of homogeneity and crystallinity and rectification ratio and barrier height approach a constant value.

Table 3
Device parameters for NiPc Schottky diode solar cells under standard illumination at 1 kW/m^2.

Annealing temperature (°C)	Open circuit voltage V_{OC} (V)	Short circuit current density J_{SC} (mA/cm^2)	Fill factor (FF)	Power conversion efficiency η ($\times 10^{-3}$)%
25	0.48	0.050	23.89	5.5
70	0.49	0.056	24.22	7.3
100	0.52	0.058	24.48	7.9
120	0.54	0.065	26.26	8.6
150	0.55	0.070	26.49	9.3

3.2.2. *Photovoltaic properties*

Fig. 10 shows the plots of current density versus voltage for ITO/PEDOT:PSS/NiPc/Al Schottky diodes under illumination. The solar cell parameters for Schottky diodes such as open circuit voltage (V_{oc}), short circuit current density (J_{sc}), fill factor (FF) and the power conversion efficiency (η) were estimated and shown in Table 3. It was observed that by increasing the annealing temperature there was an increase in the short circuit current density (J_{sc}) and open-circuit voltage (V_{oc}).This can be attributed to structural modifications of samples by annealing and increase of charge carrier concentration by illumination inducing balanced carrier mobility and minimum exciton loss. Thus, increasing the exciton recombination rate during the illumination as well as improving crystallinity and homogeneity obtained through annealing led to observed intensification of J_{sc} and V_{oc}. Consequently, film annealed at 150 °C showed the highest J_{sc} (0.070 mA/cm^2) and V_{oc} (0.55 V) values.

4. Conclusion

In summary, the structural and optical properties of NiPc thin films prepared by thermal vapor deposition and annealed in different temperatures have been investigated. Structural analysis showed that crystallization of NiPc films improved and grain size became larger as a result of the increased annealing temperature. Also, AFM analysis indicated that uniformity and morphological stability of films enhanced by annealing temperature and the film annealed

at 150 °C showed the minimum value of RMS roughness compared to other films. Direct band gap energy decreased by increasing annealing temperature up to 120 °C and varied only slightly thereafter. Finally, Schottky diodes were prepared based on NiPc films and it was found that optoelectronical characteristics of diodes were sensitive to annealing temperature variation of films. The dark current density–voltage characteristics of devices showed thermionic emission and SCLC with exponential trap distribution mechanisms dominated in the diodes at low and high applied voltages, respectively. The SCLC regime with filled traps obtained for the film annealed at 150 °C. Furthermore, photovoltaic properties of diodes under illumination showed that V_{oc} and J_{sc} values of film annealed at 150 °C (0.55 V and 0.070 mA/cm^2, respectively) were higher than those of other annealed films.

Acknowledgment

Authors are thankful to the Najafabad Branch, Islamic Azad University Research Council for the partial support of this research.

References

[1] M.D. Pirriera, J. Puigdollers, C. Voz, M. Stella, J. Bertomeu, R. Alcubilla, Journal of Physics D: Applied Physics 42 (2009) 145102–145107.
[2] C.C. Regimol, C.S. Menon, Materials Science-Poland 25 (2007) 649–655.
[3] P. Kalugasalam, D.S. Ganesan, International Journal of Engineering Science and Technology 2 (2010) 1773–1779.
[4] H.S. Soliman, M.M. El-Nahass, A.M. Farid, A.A.M. Farag, A.A. El-Shazly, The European Physical Journal-Applied Physics 21 (2003) 187–193.
[5] H.S. Soliman, A.M.A. El-Barry, N.M. Khosifan, M.M. El Nahass, The European Physical Journal-Applied Physics 37 (2007) 1–9.
[6] S. Riad, Thin Solid Films 37 (2000) 253–257.
[7] A.M. Saleh, A.O. Abu-Hilal, R.D. Gould, Current Applied Physics 3 (2003) 345–350.
[8] A.M. Saleh, A.K. Hassan, R.D. Gould, Journal of Physics and Chemistry of Solids 64 (2003) 1297–1303.
[9] F. Young, M. Shtein, S.R. Forrest, Nature Materials 4 (2005) 37.
[10] S. Sönmezoğlu, R. Taş, S. Akın, M. Can, Applied Physics Letters 101 (2012) 253301–253304.
[11] J. Yang, K.C. Gordon, Chemical Physics Letters 375 (2003) 649–654.
[12] S. Sönmezoğlu, S. Şenkul, R. Taş, G. Çankaya, M. Can, Thin Solid Films 518 (2010) 4375–4379.
[13] S. Sönmezoğlu, S. Şenkul, R. Taş, G. Çankaya, M. Can, Solid State Sciences 12 (2010) 706–711.
[14] D.X. Wang, Y. Tanaka, M. Iizuka, S. Kuniyoshi, S. Kudo, K. Tanaka, Japanese Journal of Applied Physics 18 (1999) 256.
[15] D. Gu, Q. Chen, J. Shu, X. Tang, F. Gan, S. Shen, et al., Thin Solid Films 257 (1995) 88–93.
[16] M. Pfeiffer, A. Beyer, B. Plönnigs, A. Nollau, T. Fritz, K. Leo, D. Schlettwein, S. Hiller, D. Wöhrle, Solar Energy Materials and Solar Cells 63 (2000) 83–99.
[17] H.R. Kerp, H. Donker, R.B.M. Koehorst, T.J. Schaafsma, E.E. van Faassen, Chemical Physics Letters 298 (1998) 302–308.
[18] S. Radhakrishnan, S.D. Deshpande, Sensors 2 (2002) 185.
[19] S.L.M. Van Mensfoort, R.J. De Vries, V. Shabro, H.P. Loebl, R.A.J. Janssen, R. Coehoorn, Organic Electronics 11 (2010) 1408–1413.
[20] Y.H. Lee, W.J. Kim, T.Y. Kim, J. Jung, J.Y. Lee, H.D. Park, T.W. Kim, J.W. Hong, Current Applied Physics 7 (2007) 409–412.
[21] C.J. Liu, J.J. Shih, Y.H. Ju, Sensors and Actuators B 99 (2004) 344–349.
[22] S. Karan, B. Mallik, Solid State Communications 143 (2007) 289–294.
[23] T.S. Shfai, T.D. Anthopoulos, Thin Solid Films 398 (2001) 3617.
[24] A. Twarowski, Journal of Chemical Physics 77 (1982) 4698.
[25] K.N. Narayanan Unni, C.S. Menon, Materials Letters 45 (2000) 326–330.
[26] B.D. Cullity, Elements of X-ray Diffraction, second edition, Addison-Wesley, MA, 1978 (chapter 9).
[27] S. Akın, S. Sönmezoğlu, Materials Technology: Advanced Performance Materials 27 (5) (2012) 342–349.
[28] M. Gasemi, H.R. Fallah, M. Mostajaboddavati, R. Ghasemi, A. Hassanzadeh, Solar Energy Materials and Solar Cells 98 (2012) 379–384.
[29] S. Sönmezoğlu, G. Çankaya, N. Serin, Materials Technology: Advanced Performance Materials 27 (3) (2012) 251–256.
[30] M.M. El-Nahass, K.F. Abd-El-Rahman, A.A. Al-Ghamdi, A.M. Asiri, Physica B 344 (2004) 398.
[31] Z.H. He, G. Zhao, G. Han, Physica Status Solidi A 203 (2006) 518.
[32] J. Jiang, Functional Phthalocyanine Molecular Materials, Springer, 2010.
[33] R. Azimirad, O. Akhavan, A.Z. Moshfegh, Journal of The Electrochemical Society 153 (2006) 11–16.
[34] D.S. Kim, S.Y. Kwak, Applied Catalysis A: General 323 (2007) 110–118.
[35] S. Sönmezoğlu, Applied Physics Express 4 (2011) 104104–104107.
[36] M. Neghabi, A. Behjat, Current Applied Physics 12 (2012) 597–601.